

1 **Satellite-derived direct radiative effect of biomass**
2 **smoke over broken low clouds**

3
4

5 **D. Chand*¹, R. Wood¹, T. L. Anderson¹, S. K. Satheesh^{2,3},**

6 **R. J. Charlson¹**

7 1. Department of Atmospheric Science, University of Washington, Seattle, WA, USA.

8 2. Indian Institute of Science, Bangalore, India.

9 3. NASA GSFC, Greenbelt, MD, USA.

10

11

12 * Corresponding author (duli@atmos.washington.edu Fax: +1 206 685 9302)

13

14 **December 12, 2008**

15

16

1 **Smoke from biomass burning exerts a radiative forcing on climate by reflecting and**
2 **absorbing solar radiation. For a given aerosol type and surface albedo, the**
3 **combined effects produce either a net cooling or a net warming. Here, we use a new,**
4 **satellite-based approach to quantify the top-of-atmosphere direct radiative effect of**
5 **aerosol layers advected over the partly cloudy boundary layer in the region of the**
6 **southeastern Atlantic Ocean during July-October, 2006-2007. We demonstrate that**
7 **the radiative forcing efficiency at top-of-atmosphere is primarily controlled by the**
8 **fractional area coverage of underlying clouds. This relationship is nearly linear**
9 **such that it is possible to define a critical cloud fraction at which the radiative**
10 **forcing efficiency changes sign. For this region and time period, critical cloud**
11 **fraction is about 0.4, with strong sensitivity to aerosol single scattering albedo and**
12 **underlying cloud albedo. The regional-mean direct radiative effect is three times**
13 **higher when spatial covariation between cloud cover and aerosol loading is taken**
14 **into account. These results demonstrate the importance of cloud prediction for**
15 **accurate quantification of aerosol direct effects.**

16

17

18

19

1 Biomass burning aerosols make a significant but poorly quantified contribution to
2 anthropogenic radiative forcing of climate^{1,2,3} and may affect regional atmospheric
3 circulation⁴. The most significant differences between model estimates of the top-of-
4 atmosphere (TOA) direct climate forcing (DCF) are in regions where biomass burning
5 aerosol dominates the forcing³. The DCF is the change in top of atmosphere direct
6 radiative effect (DRE_{toa}) since pre-industrial times and cannot be determined from
7 modern measurements alone⁵. Both DRE_{toa} and the absorption within the atmosphere
8 DRE_{atm} are sensitive to both aerosol optical properties (chiefly aerosol optical thickness
9 τ , absorption and size distribution)⁶, and also to the albedo of the underlying surface^{7,8}.
10 In the absence of clouds, DRE is negative over the ocean due to its low surface albedo
11 even when the aerosol is strongly absorbing⁹. However, when absorbing aerosol layers
12 are located above clouds, DRE_{toa} can be positive^{2,10}. While a few modeling studies have
13 attempted to quantify the regional effects of clouds on DRE, e.g.,¹⁰, for the first time we
14 use spaceborne lidar observations of aerosols above clouds together with observed cloud
15 optical properties to quantify the aerosol DRE and the effects of clouds upon it.

16 Previous intensive observational studies of biomass burning aerosol conducted
17 during field campaigns over North and South America^{11, 12, 13}, and over Africa^{14, 15} are
18 limited either in time or space. Passive remote sensing of aerosol optical properties is
19 routinely conducted at numerous surface sites around the globe (e.g. AERONET project
20 ¹⁶) and from satellites^{17, 18, 19}, but such approaches fail or are highly biased in presence of
21 clouds^{18, 20}, which severely limits our ability to quantify the radiative effects of aerosols
22 in regions where aerosols are advected over low level clouds.

1 Here, we quantify the optical depth τ and Angstrom exponent α of aerosol layers
2 overlying optically thick clouds over the southern Atlantic Ocean using spaceborne lidar
3 observations from ‘Cloud-Aerosol Lidar and Infrared Pathfinder Satellite Observation’
4 (CALIPSO) using the retrieval method by Chand et al.²¹. An elevated layer is here
5 defined as being a layer with a detectable optical thickness overlying a strongly
6 attenuating cloud that has a top below 3 km, although over much of the domain the low
7 cloud top height is significantly lower than this (see supplementary Figure 1 on the
8 heights of the cloud and elevated aerosol layers). For the elevated aerosol layers we use
9 the CALIPSO layer identification algorithm²¹ to determine the aerosol layer top and base
10 height. Most elevated aerosol layer top heights fall between 2.5-5.5 km and have a mean
11 thickness of approximately 2 km. Most of the clouds (86 %) are observed below 3 km
12 over the entire domain. The mode of the cloud base and top of these low level clouds are
13 about 0.7 km and 1.3 km, respectively. If the uppermost cloud layer is above 3 km the
14 aerosol optical thickness is assumed to be zero for the purposes of the radiative transfer
15 calculations. Other data-selection details are given in the Method section and in Chand et
16 al.²¹.

17 Figure 1 shows an example of the vertical and along-track structure of clouds and
18 elevated aerosol layers during a night time CALIPSO pass in August 2006. Our aerosol
19 retrieval algorithm indicates that the τ of the elevated aerosol layers is in places as high as
20 1.5. The lower detection limit of the τ retrieval is estimated to be 0.07. Data from each
21 month (Jul-Oct) for years 2006 and 2007 are integrated to obtain a seasonal average over
22 the Atlantic Ocean (7.5°N-22.5°S, 17.5°E-27.5°W).

1 We use the DISORT radiative transfer model (RTM, see Methods section) to
2 estimate the DRE of elevated aerosol layers overlying clouds and for clear sky conditions
3 over land and ocean. The model inputs are the optical properties (τ , single scattering
4 albedo ϖ , \hat{a} , and asymmetry factor g) and geometrical properties (height, thickness) of
5 the elevated aerosol layer, and the albedo of the surface underlying the aerosol layer
6 (either the cloud or surface albedo).

7 For the RTM we use τ and \hat{a} from CALIPSO using a newly developed, above-
8 cloud retrieval (see Methods and reference 21). τ is retrieved at 532 nm and \hat{a} applies to
9 the wavelength dependence of τ between 532 and 1064 nm. The model results depend
10 quite strongly upon ϖ (550 nm), which cannot currently be determined from spaceborne
11 observations²². Here we use $\varpi = 0.85 \pm 0.02$ (regional mean and uncertainty) based on an
12 updated synthesis of remote and in-situ measurements during the Southern African
13 Regional Science Initiative 2000 (SAFARI 2000).²³ For reasons discussed elsewhere,²³
14 we consider this range of values more reliable than the value of 0.90 derived by Haywood
15 et al.²⁵ during this same campaign. We set $g = 0.62 \pm 0.03$ (550 nm), consistent with size
16 distributions of lab-generated and field observed biomass burning aerosols over Southern
17 Africa²⁵ and South America (Chand et al., unpublished data and reference 24).

18 The regional distribution of mean τ (Fig 2a) clearly indicates that elevated aerosol
19 layers of significant optical thickness are present over the southern Atlantic at distances
20 of well over 2000 km from the South African coast, consistent with advection by the
21 mean flow from the continental biomass burning sources^{14, 26}. Much of the advection
22 appears to be in a zonal direction consistent with the predominantly easterly winds at 600
23 hPa north of 15°S. Weak meridional advection confines most of the aerosols to south of

1 the ITCZ. The diurnal and seasonal (July-October) mean DRE of the elevated aerosol
2 layers in terms of their impact on total atmospheric column absorption (DRE_{atm} , Fig. 2b)
3 and at the TOA (DRE_{toa} , Fig. 2c), demonstrate a major impact of elevated aerosols upon
4 the radiative budget of the atmosphere and the climate system. Note that DRE_{toa} changes
5 sign reflecting the geographic variability in the underlying cloud fractional coverage C .
6 This moves the region of strongest positive DRE_{toa} some 5° or so southward from the
7 region with maximum τ towards the region with the maximum C . Conversely, the
8 DRE_{toa} just south of the equator over the ocean is reduced because the cloud fraction
9 there is much lower. These results clearly show that the pattern of cloud cover variability
10 beneath the aerosol layers has a first order impact upon the regional distribution of
11 aerosol radiative forcing.

12 The impact of the underlying cloud is more clearly demonstrated by examination
13 of the radiative forcing efficiency ($RFE_{toa}=DRE_{toa}/\tau$) of the elevated aerosol layers
14 (Figure 3). There is a remarkably strong correlation between RFE_{toa} and the monthly
15 mean value of C ($r^2=0.96$) implying that the cloud fractional coverage is an excellent
16 predictor of the mean RFE in a particular region on a monthly timescale. The RFE_{toa} for
17 clear sky conditions is inferred to be $-34 \text{ W m}^{-2} \tau^{-1}$, whereas the mean value for cloudy
18 sky is $52 \text{ W m}^{-2} \tau^{-1}$, indicating an average increase in RFE_{toa} of 0.86 W m^{-2} per unit τ for
19 1% increase in cloud cover. The critical cloud fraction C_{crit} , for which DRE_{toa} changes
20 sign, is 0.40. Based on the Terra data used herein, the average cloud coverage over this
21 region is 0.48, leading to a positive estimate for DRE_{toa} (2.4 W m^{-2}) for the region as a
22 whole. Importantly, this is three times as large as that (0.8 W m^{-2}) obtained by assuming
23 that the spatial pattern of τ (whose seasonal-regional mean value is 0.11) is independent

1 of that in C , emphasizing the importance not only of the mean cloud fractional coverage
2 but also its spatial distribution with respect to the overlying aerosol layers. There is a
3 tendency for regions with optically thick aerosol layers to be those with a fractional
4 coverage of low clouds exceeding that for the domain as a whole. Thus knowledge of the
5 domain mean cloud cover and mean aerosol optical thickness is insufficient to determine
6 the regional mean DRE, and the covariance between the two must be considered. This is
7 a stringent challenge for global climate models which exhibit considerable deficiencies in
8 their ability to represent the correct optical properties of both clouds²⁷ and aerosols³.

9 The value of C_{crit} derived herein (0.40) is sensitive to uncertainties in aerosol
10 optical properties (see Supplementary Figure 3). Increasing ω over its uncertainty range
11 of 0.83 to 0.87 leads to an increase of almost 0.1 in C_{crit} (from 0.37 to 0.47). This
12 constitutes the greatest source of explicitly estimated error in our study. Changing \hat{a} and
13 g over their uncertainty ranges (1.1-2.1 and 0.59-0.65, respectively) causes C_{crit} to vary
14 by 0.04 in each case. In contrast, shifting cloud altitude by 1.25 km had only a minor
15 effect on C_{crit} of 0.01.

16 Podgorny and Ramanathan used an RT model to estimate the top-of-atmosphere
17 radiative effect of absorbing aerosols over broken low clouds in the Indian Ocean¹⁰.
18 Assuming thick clouds and moderately absorbing aerosol ($\omega=0.90$ at 500 nm), they found
19 a similar strong dependence upon cloud fraction, but a lower value of C_{crit} (0.25) than
20 found herein (0.40). The explanation for this difference appears to be cloud albedo,
21 which is calculated from cloud optical depth within the RT models of both studies. In
22 our study, cloud albedos are 0.50 +/- 0.06 (mean and standard deviation) based on
23 MODIS-retrieved cloud optical depths of 7.8 +/- 1.8. The calculations by Podgorny and

1 Ramanathan assumed a cloud optical depth of 15, implying much higher cloud albedo
2 (close to 0.7). This would cause aerosol over cloud have a much stronger warming
3 effect, lowering the balance point, C_{crit} . We see from this comparison that accurate
4 knowledge of cloud albedo (in addition to C , τ , and ϖ) is critical to the accurate
5 determination of aerosol radiative forcing.

6 Small scale or day-to-day covariation among aerosol and underlying cloud
7 properties (assumed herein to be zero; see Methods section) constitutes an additional,
8 unknown source of error in our estimates. A recent study conducted in the same region
9 of the SE Atlantic²⁸ demonstrates covariation of τ and C . However, this finding relied
10 on retrieving both quantities from MODIS, and the authors were careful to point out that
11 the cause could be either a physical relationship or an instrumental artifact. If physical,
12 such covariation would tend to increase the warming effect of the aerosol and lower C_{crit} .
13 Covariations among other combinations of key properties (C , cloud albedo, τ , and ϖ)
14 could also be important and should be investigated in future studies.

15 . A recent comparison of global models showed that the southeast Atlantic region exhibits
16 extremely large inter-model differences in all-sky direct radiative forcing.³ Even in the
17 annual mean, the modeled values of radiative forcing over this region vary from -1 to +2
18 W m^{-2} . These estimates are poorly constrained by traditional aerosol retrievals from
19 passive remote sensing since these methods are restricted to clear-sky situations. As
20 shown herein, above-cloud aerosol retrievals from CALIPSO combined with cloud
21 retrievals from passive satellites provide a powerful new set of tools for adjudicating
22 among the discordant model estimates and, ultimately, improving understanding of
23 aerosol radiative forcing and its dependence upon underlying clouds.

24

1 **References**

- 2 1. Intergovernmental Panel of Climate Change (IPCC): The Physical Science Basis,
3 Contribution of Working Group I to the Fourth Assessment Report of the IPCC.
4 Cambridge Univ. 916 Press, New York (2007).
- 5 2. Keil, A., and Haywood, J. M. Solar radiative forcing by biomass burning aerosol
6 particles during SAFARI 2000: A case study based on measured aerosol and cloud
7 properties. *J. Geophys. Res.*, 108(D13), 8467, doi:10.1029/2002JD002315 (2003).
- 8 3. Schulz, M. et al, Radiative forcing by aerosols as derived from the AeroCom present-
9 day and pre-industrial simulations. *Atmos. Chem. Phys.*, 6, 5225-5246 (2006).
- 10 4. Ramanathan, V., and Carmichael, G. Global and regional climate changes due to black
11 carbon. *Nature Geosciences*, 1, 221-227, (2008).
- 12 5. Bellouin, N., Jones, A., Haywood, J. and Christopher, S. A. Updated estimate of
13 aerosol direct radiative forcing from satellite observations and comparison against
14 the Hadley Centre climate model. *J. Geophys. Res.*, 113, D10205,
15 doi:10.1029/2007JD009385 (2008).
- 16 6. Haywood, J. and Boucher, O., Estimates of the direct and indirect radiative forcing due
17 to tropospheric aerosols: A review. *Rev Geophys*, 38 (4), 513-543,
18 10.1029/1999RG000078, (2000).
- 19 7. Chýlek, P., and Coakley J. A. Jr., Aerosol and climate. *Science*, 183, 75-77 (1974)
- 20 8. Seinfeld, J. , Black carbon and brown clouds. *Nature Geoscience*, Vol 1, issue 1, Pages
21 15-16 (2008)

- 1 9. Satheesh, S. K. and Ramanathan, V., Large differences in tropical aerosol forcing at
2 the top of the atmosphere and Earth's surface. *Nature* Vol. 405, Issue 6782, pages 60-
3 63 (2000).
- 4 10. Podgorny, I. A. and Ramanathan, V. A modeling study of the direct effect of aerosols
5 over the Tropical Indian Ocean, *J. Geophys. Res.*, 24,097 - 24,105 (2001).
- 6 11. Fishman, J., Hoell, J. M., Bendura, R. D., McNeal, R. J. and Kirchhoff, V. W. J. H.,
7 NASA GTE TRACE-A Experiment (September - October, 1992). *J. Geophys. Res.*,
8 101, 23,865 - 23,879 (1996).
- 9 12. Kaufman, Y. J., et al., Smoke, Clouds and Radiation-Brazil (SCAR-B) experiment. *J.*
10 *Geophys. Res.*, 103, 31,783–31,808 (1998).
- 11 13 Andreae, M. O. et al., Biomass-burning emissions and associated haze layers over
12 Amazonia, *J. Geophys. Res.-Atmos.*, 93, 1509 - 1527 (1988).
- 13 14. Andreae, M. O. et al., Influence of plumes from biomass burning on atmospheric
14 chemistry over the equatorial Atlantic during CITE-3. *J. Geophys. Res.*, 99, 12,793–
15 12, 808 (1994).
- 16 15. Lindsay, J. A., et al., International Geosphere Biosphere Programme/International
17 Global Atmospheric Chemistry SAFARI-92 field experiment: Background and
18 overview. *J. Geophys. Res.*, 101, 23,521- 23,530, (1996).
- 19 16. Holben, B. N., Eck, T. F., Slutsker, I., Tanré, D., et al.: AERONET A federated
20 instrument network and data archive for aerosol characterization. *Remote Sens.*
21 *Environ.*, 66, 1-16 (1998)

- 1 17. King, M. D., Kaufman, Y. J., Menzel, W. P., and Tanre, D. Remote sensing of cloud,
2 aerosol, and water vapor properties from the moderate resolution imaging
3 spectrometer (MODIS). *IEEE Trans. Geosci. Rem. Sens.* 30(1), 2-27, (1992).
- 4 18. Remer, L.A. et al, The MODIS Aerosol Algorithm, Products, and Validation. *J.*
5 *Atmos. Sci.*, 62, 947-973 (2005).
- 6 19. Myhre, L., et al., Regional aerosol optical properties and radiative impact of the
7 extreme smoke event in the European Arctic in spring 2006. *Atmos. Chem. Phys.*, 7,
8 5899-5915 (2007)
- 9 20. Kaufman Y. J, Remer L. A, Tanre D. A critical examination of the residual cloud
10 contamination and diurnal sampling effects on MODIS estimates of aerosol over
11 ocean. *IEEE Trans. Geosci. Rem. Sens.*, 43, 2886-2897 (2005).
- 12 21. Chand, D. et al., Quantifying above-cloud aerosol using spaceborne lidar for
13 improved understanding of cloudy-sky direct climate forcing. *J. Geophys. Res.*, 113,
14 D13206, doi:10.1029/2007JD009433 (2008).
- 15 22. Mishchenko, M.I., et al., Accurate Monitoring of Terrestrial Aerosols and Total Solar
16 Irradiance: Introducing the Glory Mission. *Bull. Amer. Meteor. Soc.*, 88, 677-691
17 (2007).
- 18 23. Leahy, L. V., Anderson, T. L., Eck, T. F., and Bergstrom, R. W. A synthesis of single
19 scattering albedo of biomass burning aerosol over southern Africa during SAFARI
20 2000. *Geophys. Res. Lett.*, 34, L12814, doi:10.1029/2007GL029697 (2007).

- 1 24. Chand, D. et al., Optical and physical properties of aerosols in the boundary layer and
2 free troposphere over the Amazon Basin during the biomass burning season. *Atmos.*
3 *Chem. Phys.*, 6, 2911-2925 (2006).
- 4 25 Haywood, J. M. et al., The mean physical and optical properties of regional haze
5 dominated by biomass burning aerosol measured from the C-130 aircraft during
6 SAFARI 2000. *J. Geophys. Res.*, 108(D13), 8473, doi:10.1029/2002JD002226,
7 (2003).
- 8 26. Anderson, T. L. et al., An “A-Train” Strategy for Quantifying Direct Climate Forcing
9 by Anthropogenic Aerosols *Bull. Amer. Meteor. Soc.*, 86, 1795–1809 (2005)
- 10 27. Karlsson, J., Svensson, G., and Rodhe, H. Cloud radiative forcing of subtropical low
11 level clouds in global models. *Clim. Dyn.*, 30, 779-788 (2008).
- 12 28 Loeb, N. G. and Schuster, G. L. An observational study of the relationship between
13 cloud, aerosol and meteorology in broken low-level cloud conditions. *J. Geophys.*
14 *Res.*, 113, 10.1029/2007JD009763 (2008).
- 15 29. King M. D., Tsay, S. C., Platnick, S. E., Wang, M. and Liou, K. N. Cloud retrieval
16 algorithms for MODIS: Optical thickness, effective particle radius, and
17 thermodynamic phase. MODIS Algorithm Theoretical Basis Doc. ATBD-MOD-05,
18 NASA (1997).
- 19 30. Ricchiazzi, P., Yang, S., Gautier, C., and Sowle, D.: SBDART, A research and
20 teaching tool for plane-parallel radiative transfer in the Earth’s atmosphere. *Bull. Am.*
21 *Meteorol. Soc.*, 79, 2101 - 2114, (1998).

1

2 **Corresponding Author:**

3 Duli Chand,

4 Department of Atmospheric Science

5 Box 351640, University of Washington

6 Seattle, WA 98195

7 USA

8 Ph +1 206 685 9525, Fax: +1 206 685 9302

9 Email: duli@atmos.washington.edu

10

11

12 **Acknowledgements:**

13 This work was supported by University of Washington startup funds, NASA's CALIPSO

14 Mission (contract NAS1-99105), and the National Science Foundation (grants ATM-

15 0601177 and ATM-0205198). We acknowledge the anonymous reviewers for their

16 constructive comments and feedbacks.

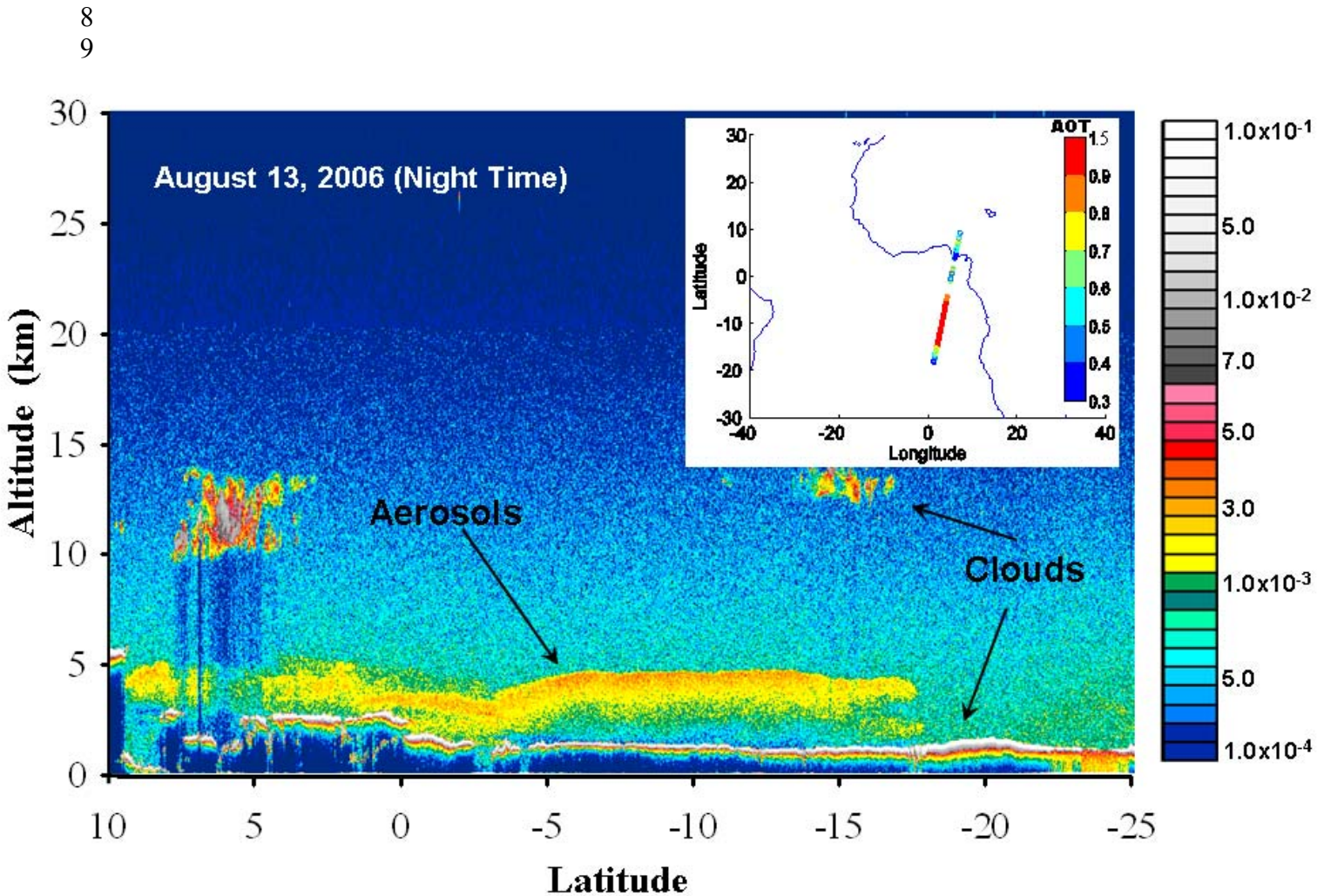
17

1 **Method**

2 Based on the active remote sensing observations from the 532 nm and 1064 nm channels
3 on Cloud-Aerosol Lidar and Infrared Pathfinder Satellite Observations (CALIPSO), we
4 developed a new method to quantify the aerosols optical depth (τ) and Ångstrom
5 exponent (\AA) of aerosol layers above clouds²⁶. Here we applied this technique regionally
6 over the southern Atlantic Ocean (7.5N-22.5S, 17.5E-27.5W) to produce monthly mean τ
7 and \AA estimates at $5^\circ \times 5^\circ$ resolution for two biomass burning seasons (July-October of
8 2006 and 2007). Data from the Moderate Resolution Imaging Spectroradiometer
9 (MODIS) on the NASA Terra satellite are used to provide monthly mean estimates of
10 ice-cloud fractional coverage (used as a data selection screen), water-cloud fractional
11 coverage C , and, water-cloud visible albedo, where the latter derives from water-cloud
12 optical thickness retrievals²⁹ and two-stream radiative transfer theory (Coakley, J.A., and
13 P. Chýlek *J. Atmos. Sci.*, 32, pp 409, 1975). Cloud data from MODIS provide essentially
14 complete coverage of each $5^\circ \times 5^\circ$ blocks every day; however, the daily, spatial coverage
15 by CALIPSO is much lower. For this reason, we use both daytime and nighttime
16 CALIPSO data and we aggregate them to monthly averages for each $5^\circ \times 5^\circ$ blocks prior to
17 combining them with MODIS data to calculate direct radiative forcing. Thus, our
18 method assumes (i) that above-cloud aerosol in this region does not exhibit significant
19 diurnal variation, (ii) that the above-cloud aerosols detected by CALIPSO along its orbit
20 are representative of the entire $5^\circ \times 5^\circ$ block, and (iii) that there is no day-to-day co-
21 variation of cloud fraction or properties with above-cloud aerosol properties. These are
22 reasonable assumptions but should be tested in follow-up studies.

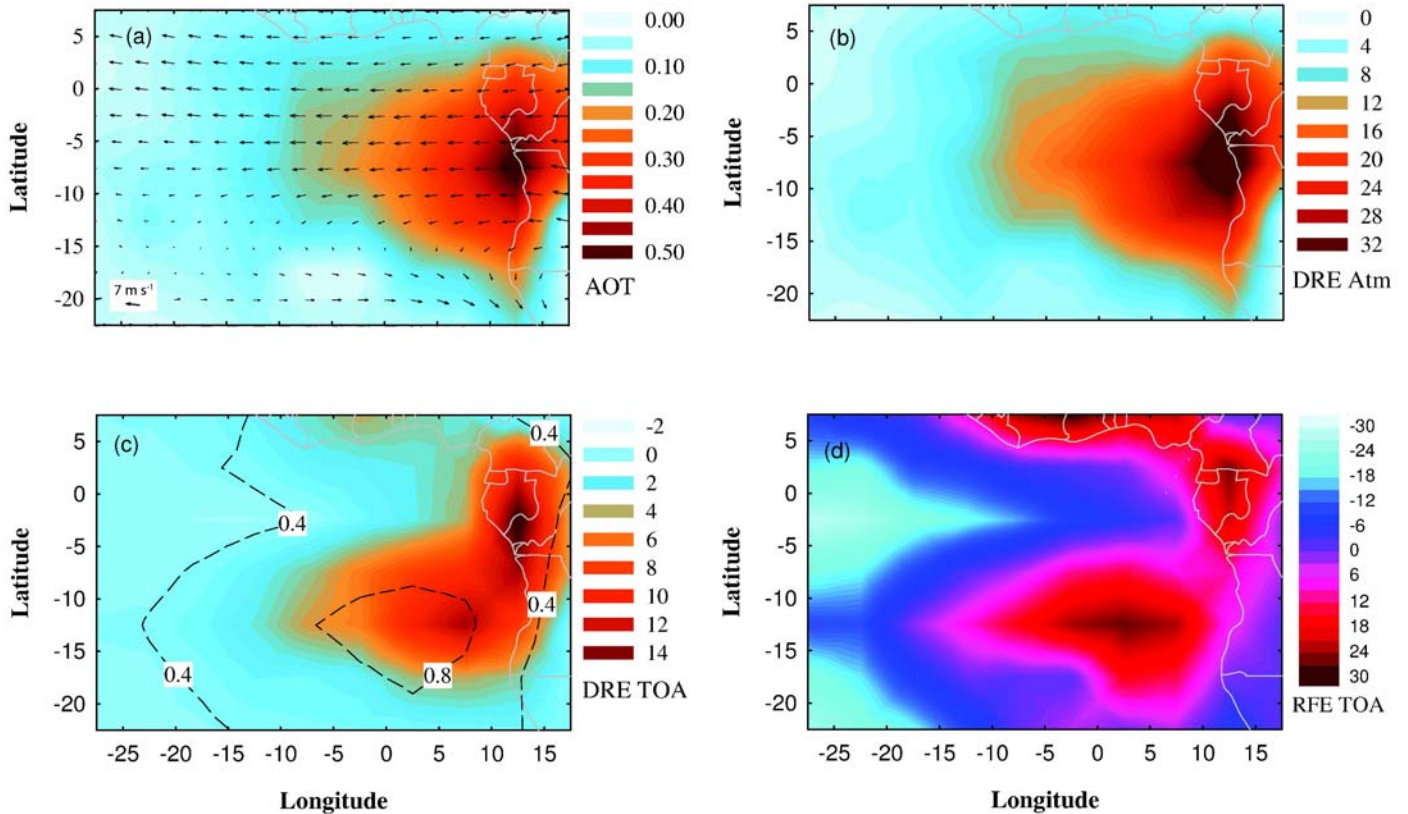
1 The direct radiative forcing efficiency (DRE) of elevated aerosol layers is
2 calculated using the DISORT radiative transfer code³⁰. Calculations are performed for
3 each 5x5 degree block at monthly-mean resolution. Because we do not explicitly model
4 the effects of cirrus clouds, blocks where ice-cloud fraction is greater than 5% were
5 excluded from the analysis. This excludes about 40% of the available blocks.
6 Calculations run without this screening are noisier (e.g. the correlation between DRE and
7 C is somewhat lower than indicated in Figure 3) but yield almost identical values of
8 domain-mean DRE and C_{crit} (see supplementary figure 4). We perform separate
9 calculations for aerosols in a clear sky situation (assuming an ocean surface albedo of
10 0.06 and a land surface albedo 0.25) and above a cloudy surface having the
11 observationally-determined mean albedo. We apply the mean cloud and aerosol heights
12 observed by CALIPSO over the entire domain. We perform additional calculations to
13 determine the sensitivity of domain-mean DRE and C_{crit} to the fixed values of ϖ , g , \hat{a} ,
14 cloud height, and aerosol height (see the supplementary figures). These calculations
15 indicate that DRE and C_{crit} are most sensitive to ϖ followed by g and \hat{a} . As long as the
16 aerosol layer is separated from the cloud layer by at least a few hundred meters, changes
17 in cloud or aerosol height have negligible effects.
18
19

1 **Figure 1 Profiles of 532nm backscatter return signal from the CALIPSO lidar**
 2 **showing the vertical distribution of aerosols and underneath clouds.** Aerosols optical
 3 thickness (AOT) is shown by the plate at right top corner. Strong backscattering (>0.001
 4 $\text{sr}^{-1} \text{ km}^{-1}$) is associated with aerosol and/or cloud layers (as indicated by arrows).
 5 Observations from 2006 and 2007 indicate that such events are very frequent during the
 6 biomass burning season (particularly August and September) over the west coast of
 7 Africa between the equator and 20°S .



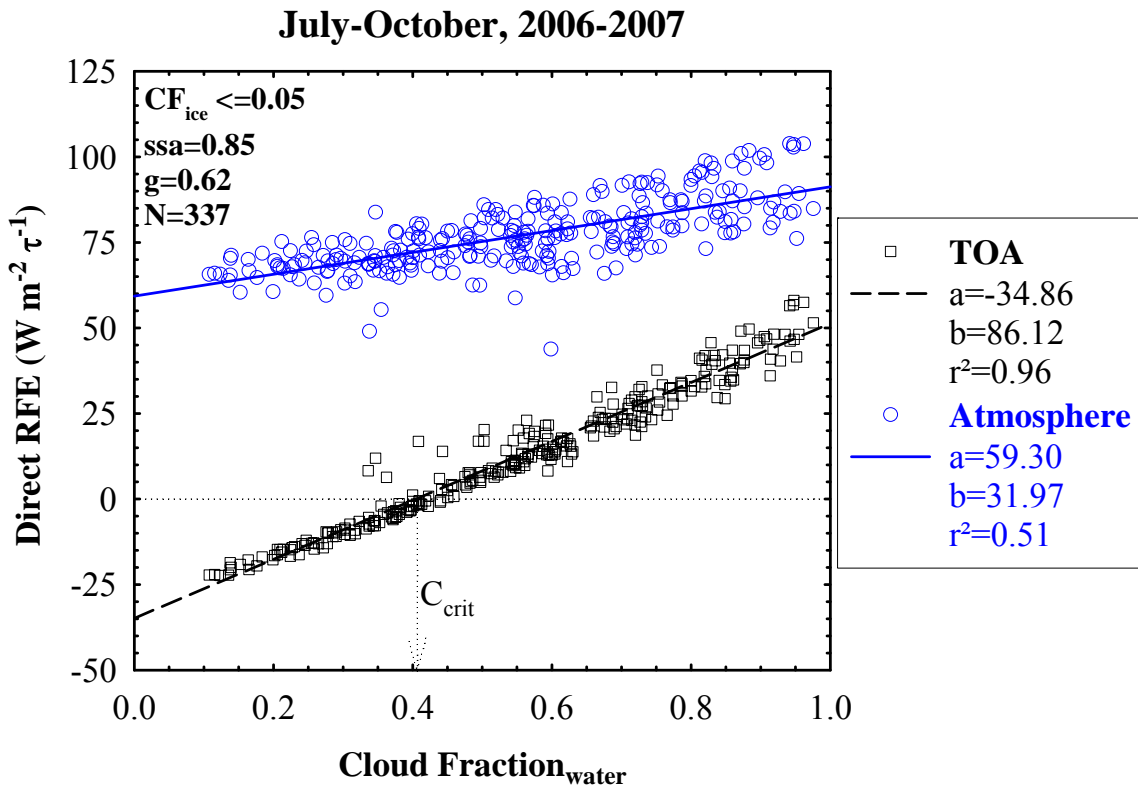
1 **Figure 2 Regional distributions of aerosols and its radiative impacts with winds and**
 2 **cloud fraction.** Maps showing seasonal (July-October, 2006/2007) mean values of: (a)
 3 aerosol optical thickness τ (including zeros when no elevated aerosol layer is detected),
 4 and National Centers for Environmental Prediction (NCEP) winds at 600 hPa; (b)
 5 Atmospheric direct radiative effect (DRE_{atm} ; column absorption); (c) Direct radiative
 6 effect at top of the atmosphere (DRE_{toa} shown by colors and cloud fraction shown by
 7 contour lines); and (d) the direct radiative forcing efficiency, RFE ($RFE=DRE_{toa}/\tau$). The τ
 8 and cloud fraction are retrieved from CALIPSO satellite and MODIS-Terra satellite,
 9 respectively.

10
 11



1 **Figure 3 Correlation of aerosol direct radiative forcing efficiency (RFE) with cloud**
 2 **fraction.** Radiative forcing efficiency at top of the atmosphere (squares), and within the
 3 atmosphere (circles) as a function of cloud fraction. C_{crit} Is the cloud fraction when the
 4 top of atmosphere (TOA) RFE changes sign.

5
 6
 7



8
 9

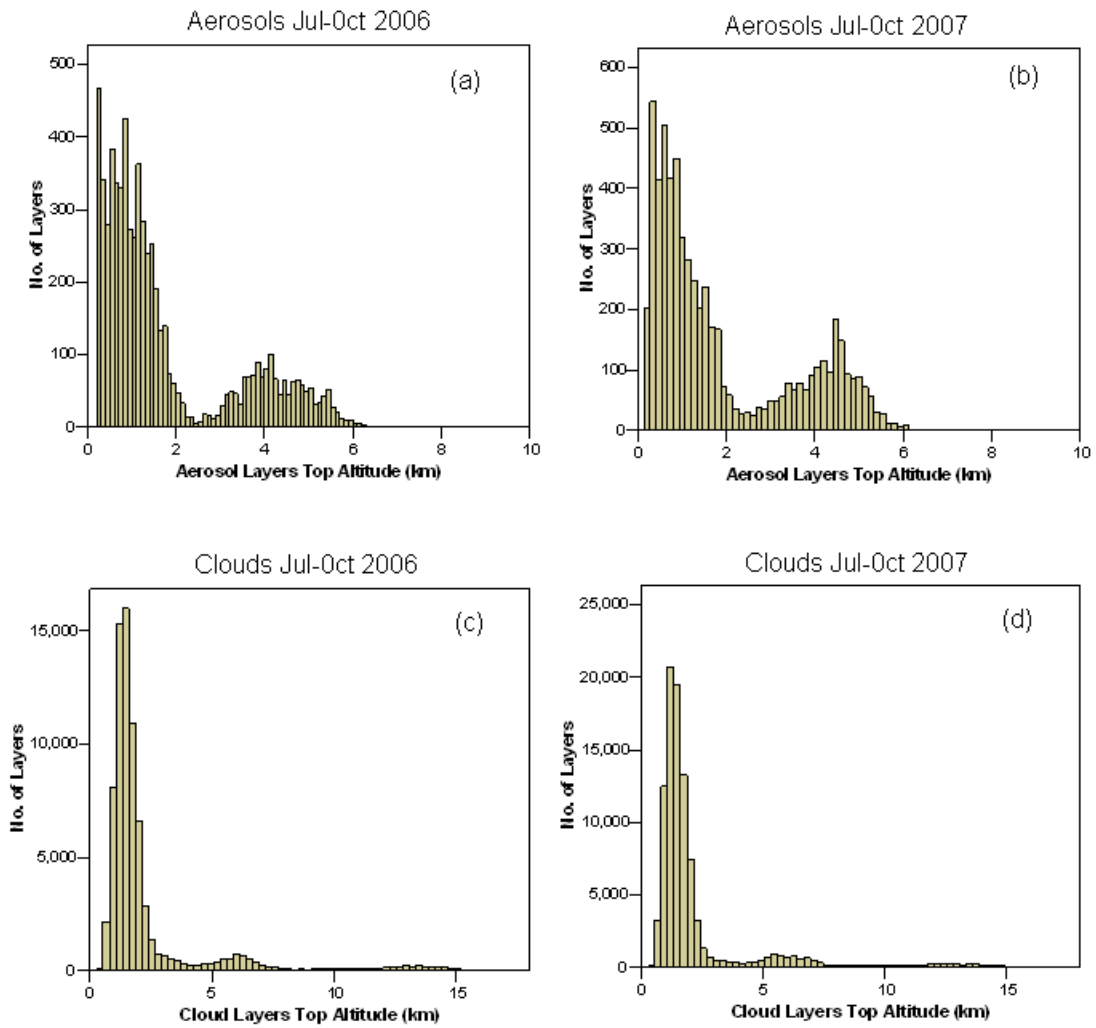
1 **Supplementary Figure 1 Frequency distribution of aerosol and underneath clouds.**

2 Histograms of the top and bottom altitudes of aerosol layers (a, b) and cloud layers (c, d).

3

4

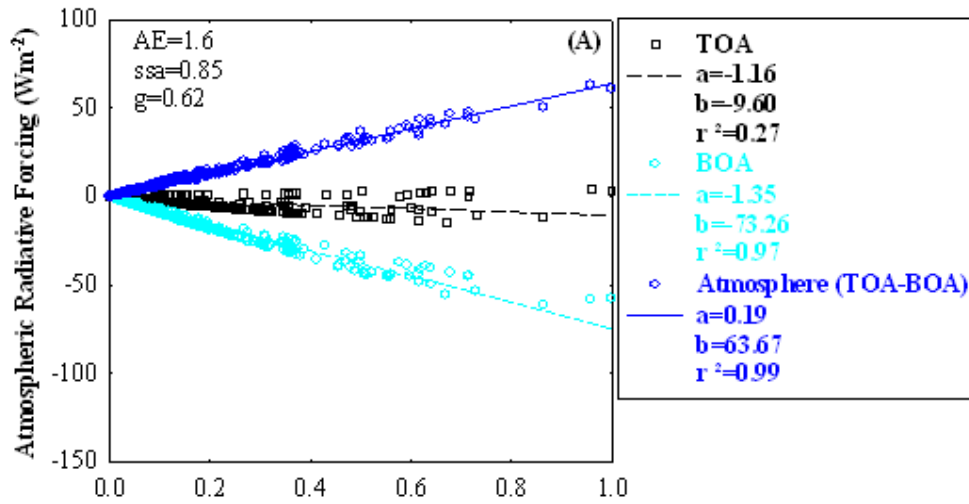
5



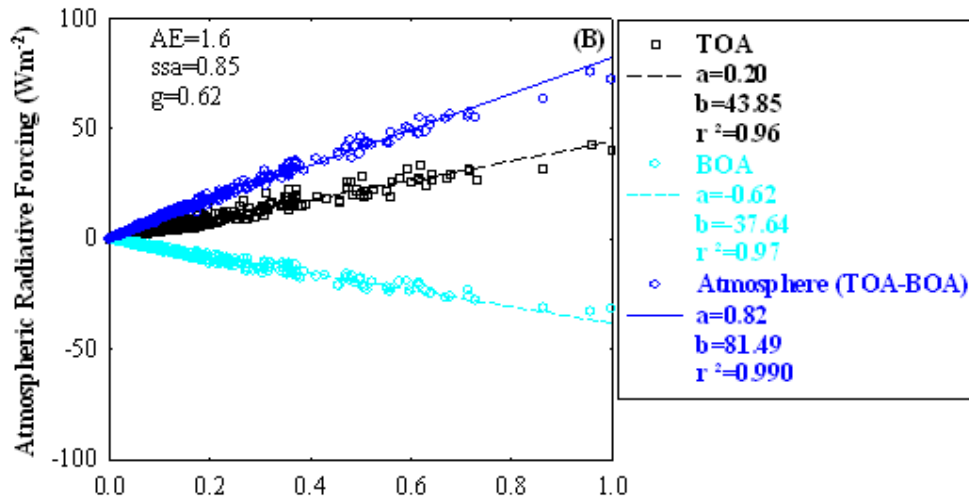
6

1 **Supplementary Figure 2 Atmospheric radiative forcing by ‘above-cloud’ aerosols**
2 **for clear, cloudy and all sky conditions.** Scatter plots of aerosols optical depth (AOD)
3 w.r.t. radiative forcing at the top of the atmosphere (TOA), bottom of the atmosphere
4 (BOA) and within the atmosphere (TOA-BOA) for (A) clear sky conditions (A); (B)
5 cloudy sky conditions; and (C) all sky conditions. The text in the right side boxes shows
6 the intercepts, slopes and correlation coefficient (r^2) of the regression lines. The radiative
7 model is run using angstrom exponent (AE)=1.6, single scattering albedo (ssa)=0.85 and
8 asymmetry factor (g)=0.62; as shown on the top right corners of the respective plates.
9 The equations shown at the bottom of the panel (C) are used to get the radiative forcing at
10 TOA and BOA in all sky conditions.
11

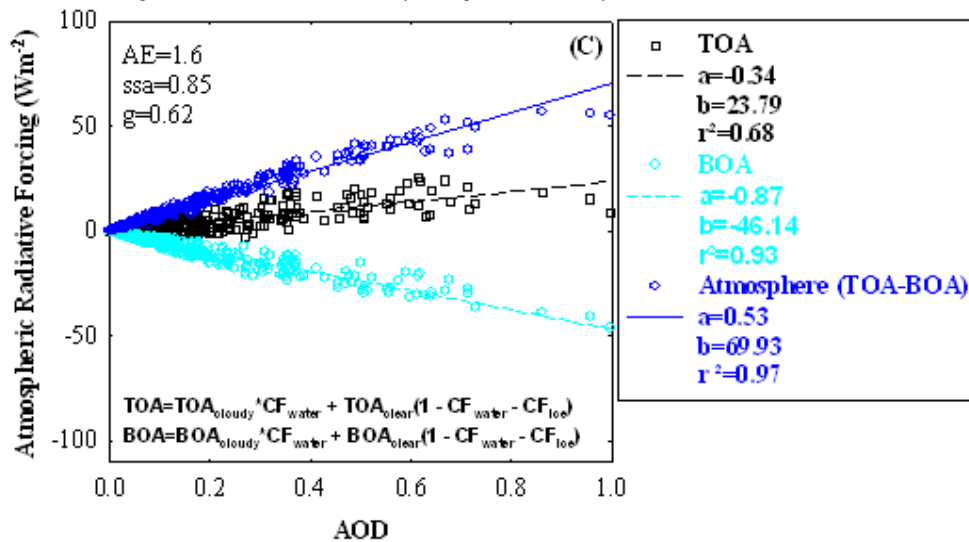
July-October, 2006-2007 (clear sky conditions)



July-October, 2006-2007 (cloudy conditions)

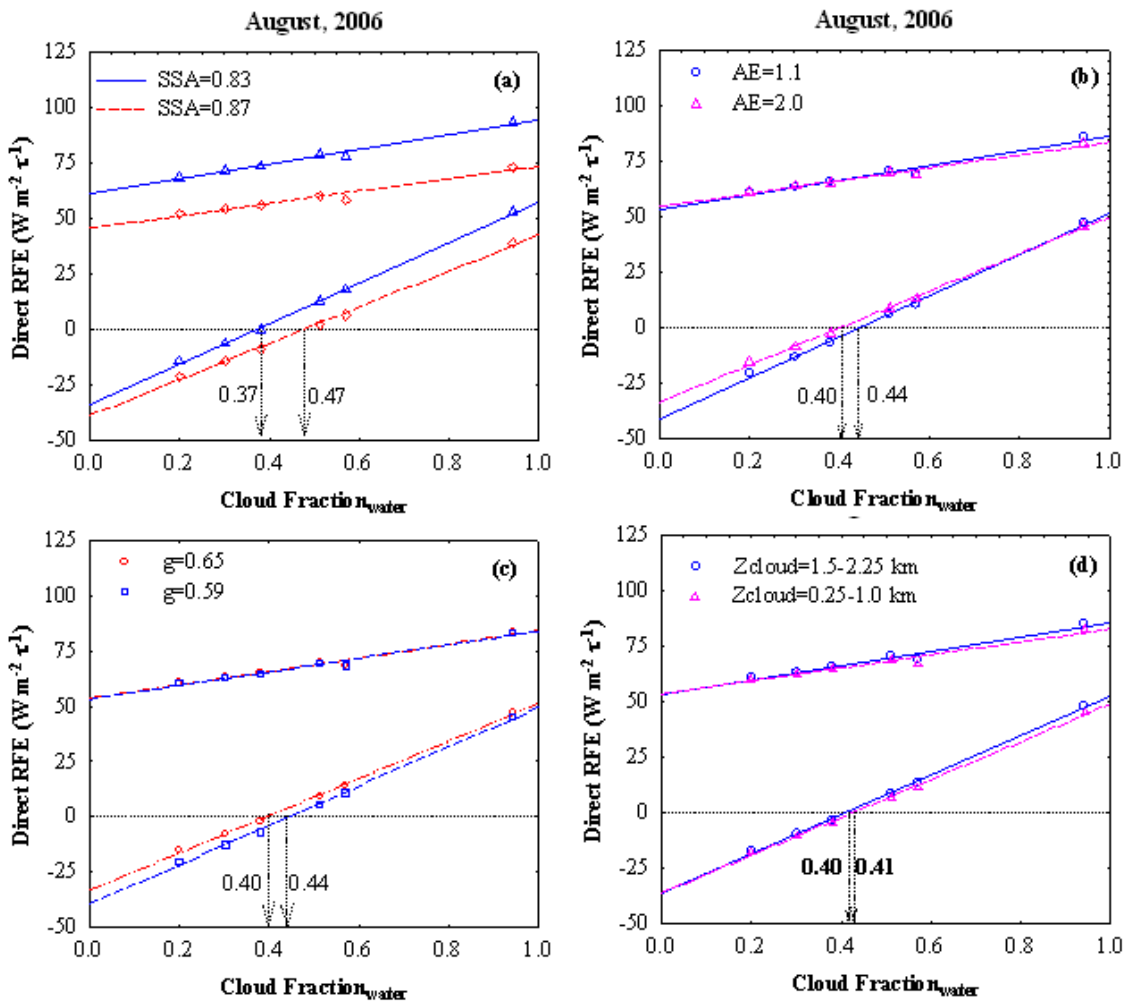


July-October, 2006-2007 (all sky conditions)



1 **Supplementary Figure 3. Sensitivity of aerosol direct radiative forcing efficiency to**
 2 **changes in aerosol and cloud properties.** Scatter plots of water cloud fraction with
 3 respect to direct radiative forcing efficiency (RFE) showing sensitivity at the top of the
 4 atmosphere (TOA) and within the atmosphere. The sensitivity is derived by varying (a)
 5 single scattering albedo (ssa); (b) angstrom exponents (AE); (c) asymmetry factors (g);
 6 and (d) cloud top altitude (Zcloud). The vertical arrows show the impact on critical water
 7 cloud fraction (C_{crit}) at the top of the atmosphere when the parameter in equation is
 8 changed. In each plate the lower two regressions are for RFE at TOA and the upper two
 9 are for the RFE within the atmosphere.

10
 11



12
 13

1 **Supplementary Figure 4. Correlation of aerosol direct radiative forcing efficiency**
 2 **(RFE) with liquid water cloud and cirrus (ice) cloud fraction.** Scatter plots of water
 3 cloud fraction with respect to direct radiative forcing efficiency (RFE) at the top of the
 4 atmosphere (TOA) and within the atmosphere for different data screening criteria based
 5 on ice cloud fraction CF_{ice} (a) $CF_{ice} \leq 1$, (b) $CF_{ice} \leq 0.2$, (c) $CF_{ice} \leq 0.1$ and (d) $CF_{ice} \leq 0.05$.
 6 The text in the right sides boxes of the plates show the intercepts, slopes and correlation
 7 coefficients (r^2) of the regression lines. The radiative model is run using angstrom
 8 exponent (AE)=1.6, ssa=0.85 and asymmetry factor (g)=0.62; as shown on the top right
 9 corners of the respective plates. The value of ice cloud fraction (CF_{ice}) used for the
 10 screening and number of data points (N) are also shown on the top-left corners of the
 11 plates.
 12
 13

